

# Quantum information analysis of electronic states at different molecular structures

G. Barcza and Ö. Legeza

*Fachbereich Physik, Philipps-Universität Marburg, 35032 Marburg, Germany  
Research Institute for Solid State Physics, H-1525 Budapest, P. O. Box 49, Hungary*

K. H. Marti and M. Reiher

*Laboratorium für Physikalische Chemie, ETH Zurich, 8093 Zurich, Switzerland*

(Dated: Wed Aug 25 10:58:17 CEST 2010)

We have studied transition metal clusters from a quantum information theory perspective using the density-matrix renormalization group (DMRG) method. We demonstrate the competition between entanglement and interaction localization. We also discuss the application of the configuration interaction based dynamically extended active space procedure which significantly reduces the effective system size and accelerates the speed of convergence for complicated molecular electronic structures to a great extent. Our results indicate the importance of taking entanglement among molecular orbitals into account in order to devise an optimal orbital ordering and carry out efficient calculations on transition metal clusters. We propose a recipe to perform DMRG calculations in a black-box fashion and we point out the connections of our work to other tensor network state approaches.

## I. INTRODUCTION

The most important property of multi-component quantum systems is entanglement which corresponds to quantum correlations between particles or a collection of particles forming a larger subsystem [1]. The degree of entanglement is decisive for the behavior of all multi-component quantum systems and for the numerical algorithms developed to simulate such systems [2–11].

The concepts of quantum information theory (QIT) have been introduced to the density matrix renormalization group (DMRG) method [2, 3] and created a fresh impetus to the development of new methods that focus on entanglement optimization [12, 13]. It was shown that the quantum information entropy is a direct measure of the behavior of quantum systems. Thus, it is mandatory to develop methods and techniques to obtain as much information as possible from entropy analyses [13–18].

Since the first application of the DMRG algorithm to quantum chemical systems using the full electronic Hamiltonian [19], the method has gone through major algorithmic developments by various groups [20–24]. In 2002, two groups independently provided the first large scale calculations on diatomic molecules [25, 26]. Calculations on the  $F_2$  molecule by keeping more than 2000 block states (i.e., states defined on the active subsystem in DMRG) denoted as  $M$  in the following, and on the water molecule using 6000 block states [27] confirmed that the DMRG method is capable of reaching the limit of the full-CI method in cases where most standard quantum chemical approaches fail and cannot be applied due to the requirement of very large active spaces. Efficient calculations of excited states and the relation between the DMRG wave function and the standard CI-expansion have already been discussed in Ref. [28]. The authors have also shown that the DMRG wave function is also suited to study problems when the characteristics of the wave function changes drastically, for exam-

ple, when the bond length between diatomic molecules is changed. Therefore, it became evident that very accurate results can be obtained by increasing the computational resources related to the DMRG block states. On the other hand, the more important questions, namely what is the minimum computational effort to obtain results with a given accuracy is still unsolved and part of active research [14, 16, 22, 29].

A key-ingredient of the DMRG method related to its multi-component subsystem wave function representation is entanglement. A controlled manipulation of it is expected to extend capabilities of DMRG to treat larger systems in a more efficient way. The development of entanglement reduction algorithms (ERA) is thus very appealing. Matrix product states (MPS) [30] that are inherently produced by the DMRG algorithm can be used to localize the entanglement by reordering sites [13, 15, 25, 26, 31] or by optimization of the basis [11, 16, 29, 32–37]. Considering the entanglement between arbitrarily chosen pairs of sites [10, 15], a network topology can be determined for tensor-network-state (TNS) algorithms [11]. Further gain in speed of convergence can be achieved by an optimization of the initialization procedure [13, 38] in which highly entangled states are taken into account from the very beginning. One such algorithm is the dynamically extended active space (DEAS) method [13], and its extension by including CI-expansion techniques (CI-DEAS) [39, 40]. In this article, we will show that the proposed entropy-based optimization scheme including the (CI-)DEAS and the dynamic block state selection (DBSS) procedures are vital ingredient to obtain highly accurate results with tremendous savings in computation resources and time. In addition, it is a smart way of reducing the Hilbert space which allows us to study large active spaces with a modest number of renormalized states in contrast to inefficient and expensive brute-force DMRG calculations at a fixed number of renormalized states. DMRG cal-

culations on complex chemical systems using quantum information theory have not yet been carried out, and are the subject of this work.

The very challenging binuclear oxo-bridged copper clusters identified in Ref. [41] as a very difficult case for complete-active-space-like calculations pose an ideal test for the DMRG algorithm. In a pioneering study, some of us investigated the DMRG algorithm for the prediction of relative energies of transition metal clusters of different molecular structures, the bis( $\mu$ -oxo) and  $\mu - \eta^2 : \eta^2$  peroxy isomers of  $[\text{Cu}_2\text{O}_2]^{2+}$  [42]. Based on these results, we drew the conclusion that the DMRG algorithm is suited to study transition metal complexes and clusters. Kurashige and Yanai have picked up that same problem as well and performed massively parallel DMRG calculations employing 2400 renormalized basis states but on a larger active space with a smaller one-particle basis [43]. In their study, a new aspect was the inclusion of a perturbative correction introduced originally by White [44] for the one-site DMRG algorithm to prevent convergence to local minima during the optimization process. In the present study of  $[\text{Cu}_2\text{O}_2]^{2+}$ , we show that no convergence acceleration technique such as white noise [25] or perturbative correction [43] is needed if an entropy-based optimization scheme is employed.

The purpose of the paper is to show how quantum information entropies can be efficiently exploited to perform accurate calculations on complicated chemical systems such as transition metal clusters. Our results indicate that – within chemical accuracy – much larger molecular systems can be studied than before using very little computational resources. In Sec. III, we briefly discuss the various technical aspects of our calculations while the entropy analysis of the two isomers are presented in Sec. IV. In Sec. V, extensions to tensor network state methods are discussed and our conclusions are given.

## II. THE CHALLENGE OF BINUCLEAR COPPER CLUSTERS

The reliable first-principles description of transition metal complexes and clusters remains an important task for theoretical molecular physics and quantum chemistry — especially because of the role of such molecules in catalysis and bioinorganic chemistry [45–48].

In 2006, Cramer *et al.* investigated several theoretical models on the  $[\text{Cu}_2\text{O}_2]^{2+}$  torture track and found incisive discrepancies between them [41]. The CASSCF calculations even yield a qualitatively wrong interpretation of the energy difference between the two isomers. The reason for this striking failure lies in the inability of the CASSCF method to include all relevant molecular orbitals into the one-particle active space that would be necessary to obtain a qualitatively correct description of the electronic structure. Already the qualitative picture of an extended Hückel calculation indicated the require-

ment of more than doubling the active space for binuclear transition metal clusters compared to the mononuclear analog [42]. An additional support for the fact that a very large active space is needed for a correct description of the electronic structure of transition metals is the finding of Pierloot *et al.* to include a second  $d$  shell to obtain accurate results [49]. As we showed in our previous work [42], the DMRG algorithm is an ideal candidate to tackle the description of challenging electronic structures that require large active spaces occurring in transition metal chemistry.

This work reinvestigates the dicopper clusters with an improved methodology transforming the DMRG approach eventually into a black-box method with significantly reduced computational requirements. For our DMRG calculations, the same active space, one-particle basis set and effective core potential as in Ref. [42] was used. All quantities calculated in this paper will be given in Hartree atomic units of which the energy unit is one Hartree.

## III. NUMERICAL PROCEDURE

In this section, we outline the procedures and methods needed for the entropy-based optimization scheme to efficiently carry out DMRG calculations. Examples and figures will be presented for the  $\mu - \eta^2 : \eta^2$  peroxy isomer of  $[\text{Cu}_2\text{O}_2]^{2+}$  while for the bis( $\mu$ -oxo) isomer only the final results are given.

### A. Molecular Hamiltonian in second quantization

In quantum chemical (QC-)DMRG applications, the electron–electron repulsion is taken into account by an iterative procedure that minimizes the Rayleigh quotient corresponding to the electronic Hamiltonian given by

$$H = \sum_{ij\sigma} T_{ij} c_{i\sigma}^\dagger c_{j\sigma} + \sum_{ijkl\sigma\sigma'} V_{ijkl} c_{i\sigma}^\dagger c_{j\sigma'}^\dagger c_{k\sigma'} c_{l\sigma} \quad (1)$$

and thus determines the full-CI wave function. In Eq. (1),  $c_{i\sigma}$  and  $c_{i\sigma}^\dagger$  are the usual electron annihilation and creation operators,  $T_{ij}$  denotes the one-electron integral comprising the kinetic energy of the electrons and the external electric field of the nuclei.  $V_{ijkl}$  stands for the two-electron integrals and contains the electron–electron repulsion operator, defined as

$$V_{ijkl} = \int d^3x_1 d^3x_2 \frac{\phi_i^*(\vec{x}_1) \phi_j^*(\vec{x}_2) \phi_k(\vec{x}_2) \phi_l(\vec{x}_1)}{|\vec{x}_1 - \vec{x}_2|}. \quad (2)$$

We obtain the Hartree–Fock orbitals in a given one-particle basis of atomic Gaussian functions and transform the one-electron and two-electron integrals in the atomic basis set to the Hartree–Fock molecular orbital basis using the MOLPRO program package [50], which

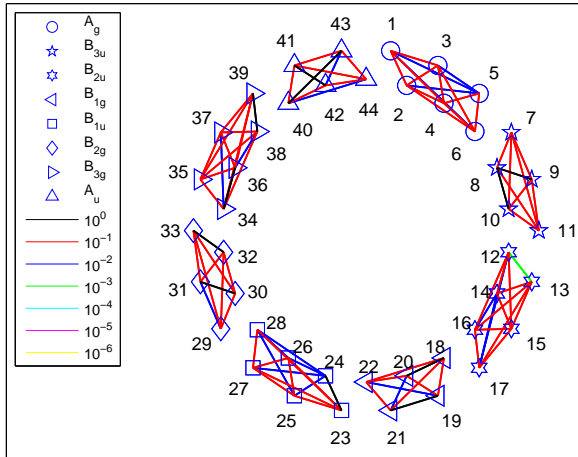


FIG. 1: (Color online) Pictorial representation of the magnitude of components  $T_{ij}$  of the one-electron operator for the  $\mu - \eta^2 : \eta^2$  peroxo isomer of  $[\text{Cu}_2\text{O}_2]^{2+}$ . For better visibility the one-dimensional orbital chain is plotted on a circle with modulated radius in a clockwise direction. Orbitals belonging to different irreducible representations are shown by different symbols. Numbers next to the symbols label molecular orbitals.

we also employ to obtain reference complete-active-space self-consistent field (CASSCF) and complete-active-space configuration-interaction (CASCI) energies.

In the QC-DMRG algorithm, a one-dimensional chain is built up from molecular orbitals obtained from a suitable mean-field or multi-configuration self-consistent field (MCSCF) calculation. As will be discussed later, the one-orbital entropy function [13] and the two-orbital mutual information [15] provide a good starting configuration. The irreducible representations of the orbitals can also be used in the DMRG procedure to carry out calculations for a given point-group symmetry [13]. This will be used in the present work, and as an example, the components  $T_{ij}$  of the one-electron operator are shown in Fig. 1 for the  $\mu - \eta^2 : \eta^2$  peroxo isomer of  $[\text{Cu}_2\text{O}_2]^{2+}$ .

## B. Two-site variant of the DMRG method

For our DMRG calculations, we employ the two-site variant of the DMRG method introduced by White [2]. In the superblock configuration, two sites are between two blocks (sets) of orbitals. To fix the notation for the rest of the paper, we label the block states of the left block containing  $l$  orbitals, the two intermediate sites and the right block with  $r$  orbitals by  $M_l, q_{l+1}, q_{l+2}, M_r$ , respectively. The total number of orbitals  $N$  is  $l + 2 + r$ . When a larger block is formed during the renormalization steps by adding a single site to the left or to the right block the new block states are denoted by  $M_L$  and  $M_R$  where  $L = l + 1$  and  $R = r + 1$ . The one-site vari-

ant of the DMRG [44] related to the MPS approach was first applied in quantum chemistry in Ref. [26] for fixed number of block states but convergence properties were found considerably worse than for the two-site DMRG algorithm. This can be improved by the introduction of a local density operator [44] which was used by Kurashige and Yanai for the calculation of the transition metal cluster compound with 2400 block states [43]. Although the size of superblock Hilbert space is smaller in this case, we use the two-site variant since this configuration allows one to control the number of block states dynamically and convergence to local minima is less likely [26].

## C. Dynamic Block State Selection

A fundamental concept related to the inseparability and non-locality of quantum mechanics is entanglement. Since the QC-DMRG algorithm approximates a composite system with long-range interactions, the results of quantum information theory can be used to understand the criteria of its convergence.

The two-site variant of the DMRG method has originally been employed with a fixed number of block states while the degree of entanglement between the DMRG blocks for a given superblock configuration is related to the Schmidt number  $r_{\text{Schmidt}}$ . For a pure target state  $|\Psi_{\text{TS}}\rangle \in \Lambda = \Lambda_L \otimes \Lambda_R$ , with  $\dim \Lambda_L = M_L$ ,  $\dim \Lambda_R = M_R$ , the Schmidt decomposition states that

$$|\Psi_{\text{TS}}\rangle = \sum_{i=1}^{r_{\text{Schmidt}} \leq \min(M_L, M_R)} \omega_i |e_i\rangle \otimes |f_i\rangle, \quad (3)$$

where  $|e_i\rangle \otimes |f_i\rangle$  form a bi-orthogonal basis  $\langle e_i | e_j \rangle = \langle f_i | f_j \rangle = \delta_{ij}$ , and  $0 \leq \omega_i \leq 1$  with the condition  $\sum_i \omega_i^2 = 1$ . If  $r_{\text{Schmidt}} > 1$  then according to Ref. [51]  $|\Psi_{\text{TS}}\rangle$  is inseparable and the two blocks are entangled.

Since possible measures of entanglement for fermionic systems are the von Neumann and Rényi entropies, it is more efficient to control the truncation error [26] or the quantum information loss  $\chi$  at each renormalization step [14]. In the DMRG procedure, during the renormalization step the block  $B_L$  is formed of the subblock  $B_l$  and the  $l+1^{\text{th}}$  site. Denoting by  $s_L(l)$  the entropy of the left subblock of length  $l$  and by  $s_{l+1}$  the entropy of the  $l+1^{\text{th}}$  site, the change of the block entropy by forming a larger block,  $B_L(l+1)$ , is given as

$$s_L(l) + s(1)_{l+1} + I_L(l) = s_L(l+1), \quad (4)$$

where the von Neumann entropy of a block with  $l$  orbitals is given as

$$s_L(l) = - \sum_{\alpha} \omega_{\alpha} \ln \omega_{\alpha}, \quad (5)$$

where  $\omega_{\alpha}$  stands for the eigenvalues of the reduced density matrix of the block  $B_l$ . The so-called mutual information  $I_L(l) \leq 0$  quantifies the correlation between the

subsystem and the site and it is zero if and only if the two blocks are uncorrelated.

In order to control the quantum information loss,  $M_L$  (or  $M_R$ ) is increased systematically at each renormalization step until the following condition holds

$$s_L(l+1) - s_L^{\text{Trunc}}(l+1) < \chi, \quad (6)$$

where  $\chi$  is an a priori defined error margin. For  $s_L(l+1)$ , i.e., before the truncation,  $\alpha = 1 \dots M_l \times q_{l+1}$  while for  $s_L^{\text{Trunc}}(l+1)$  according to Eq. (6)  $M_l^{\text{Trunc}} < M_l \times q_{l+1}$  is used. This approach guarantees that the number of block states are adjusted according to the entanglement between the DMRG blocks and the a priori defined accuracy can be reached [14]. In addition, an entropy sum rule can be used as an alternative test of convergence [14]. Therefore, we set the minimum number of block states to  $M_{\min}$  and  $\chi$ . By setting  $M_{\min} \simeq q^3$  or  $q^4$ , convergence to local minima can be avoided. In our implementation, we have  $q = 4$  and the basis states correspond to the  $|0\rangle, |\downarrow\rangle, |\uparrow\rangle$  and  $|\downarrow\uparrow\rangle$  states. The maximum number of block states selected dynamically during the course of iterations will be denoted by  $M_{\max}$ . This approach, however, does not work for the one-site variant of the DMRG algorithm since the Schmidt number of a one-site superblock configuration  $M_L = M_l \times q_{l+1}$  cannot be larger than  $M_r$ . This prevents  $M_l$  to increase above  $M_r$  according to Eq. (3).

#### D. Entanglement and interaction localization

The von Neumann and Rényi entropies have been studied for quantum chemical systems as well and it was shown that orbitals lying closer to and further away from the Fermi surface possess larger and smaller orbital entropy, respectively [13]. The orbital entropy is related to the mixture of a local state and it is expressed by the eigenvalues of the reduced density matrix for a given orbital, namely

$$s(1)_i = - \sum_{\alpha} \omega_{\alpha,i} \ln \omega_{\alpha,i}, \quad (7)$$

where  $i = 1 \dots N$  labels the orbital index while  $\omega_{\alpha,i}$  stands for  $\alpha = 1 \dots q_i$  the eigenvalues of the reduced density matrix of orbital  $i$ . In Fig. 2, the single-orbital entropy is shown for the  $\mu - \eta^2 : \eta^2$  peroxo isomer of  $[\text{Cu}_2\text{O}_2]^{2+}$  calculated by setting the quantum information loss  $\chi = 10^{-5}$ . Orbitals with a large entropy significantly contribute to the correlation energy whereas other slightly entangled orbitals do not. Since the orbitals possess different single-orbital entropies, the ordering of orbitals along the one-dimensional chain of orbitals in the DMRG algorithm has a major impact on the block entropy  $s(l)$ , so that the block entropy profile can be changed based on the ordering of the orbitals [13]. The block entropy also determines the required computational resources to reach a given accuracy [13, 14]. If

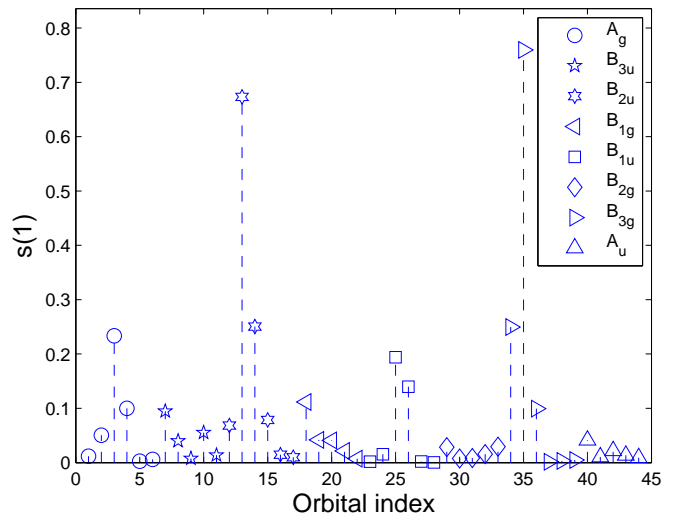


FIG. 2: (Color online) Single-orbital entropy function obtained for the  $\mu - \eta^2 : \eta^2$  peroxo isomer of  $[\text{Cu}_2\text{O}_2]^{2+}$  by setting the quantum information loss  $\chi = 10^{-5}$ . The symbols indicate corresponding point-group symmetries of the energetically ordered orbitals.

an optimized ordering is used, DMRG results can be obtained using a considerably smaller number of block states for a given error bound.

An optimal orbital alignment by means of speed of convergence can be obtained by reordering the orbitals, so that the DMRG blocks are entangled only for a few iterations. This can be achieved by placing highly entangled orbitals at one of the ends or close to the center of the chain.

Unfortunately, this is not true in general, since the independent interaction terms, like  $T_{ij}$  and the local direct, pair-hopping, and spin-flip terms of  $V_{ijkl}$  act as independent quantum channels; they all generate different amounts of entanglement [16]. Hence, localizing entanglement generated by one channel, e.g., the one-electron term, might lead to delocalized entanglement in another channel. As an example, the one-electron operators are analyzed for the  $\mu - \eta^2 : \eta^2$  peroxo isomer of  $[\text{Cu}_2\text{O}_2]^{2+}$  shown in Fig. 1. In this case they do not couple orbitals among different irreducible representations of the  $D_{2h}$  point group while the two-electron Coulomb repulsion operator does. A proper cost function to take care of interaction and entanglement localization can be expressed based on the two-orbital mutual information,

$$I_{i,j} = s(2)_{i,j} - s(1)_i - s(1)_j, \quad (8)$$

where  $s(2)_{i,j}$  is the two-orbital entropy between a pair of sites which was introduced to the QC-DMRG by Rissler *et al.* [15]. If the electron-electron interactions are neglected, the two-orbital mutual information has a similar structure as shown in Fig. 1, where only the orbitals of the same irreducible representations are entangled. The

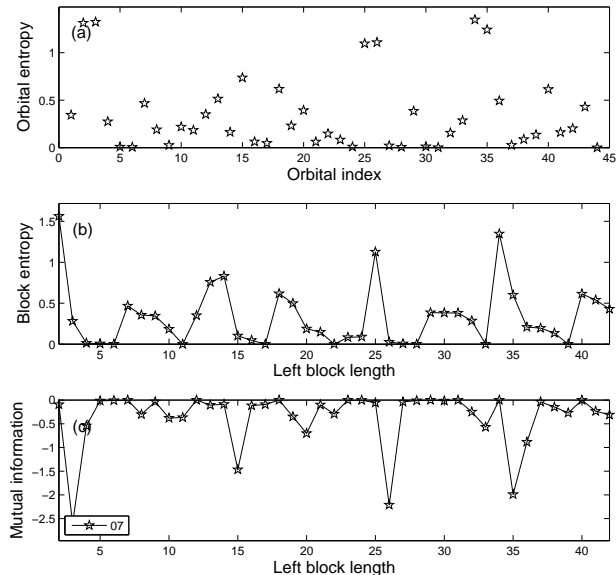


FIG. 3: (Color online) (a) The single-orbital entropy, (b) block-entropy, and (c) the mutual information obtained for the  $\mu - \eta^2 : \eta^2$  peroxo isomer of  $[\text{Cu}_2\text{O}_2]^{2+}$  after the seventh DMRG sweep while neglecting the electron–electron interactions.

resulting single-orbital entropy, block-entropy, and the mutual information are shown in Fig. 3 obtained by the DMRG method after the seventh sweep. The block entropy oscillates and is exactly zero when all orbitals of the same irreducible representations belong to the left or to the right DMRG block. Therefore, the total wave function can be expressed as a product state of the wave functions of the subblocks of irreducible representations. When the two-electron integrals are also considered, orbitals among different irreducible representations are also entangled as shown by the components of the two-orbital mutual information in Fig. 4 for the  $\mu - \eta^2 : \eta^2$  peroxo isomer of  $[\text{Cu}_2\text{O}_2]^{2+}$ . Since the one-electron integrals are usually an order of magnitude larger in chemical systems, an optimal ordering can be found by reordering the orbitals within the same irreducible representation and reordering the blocks of different irreducible representations [14, 15, 39]. In this way, the block entropy can be reduced significantly but the one-electron terms having the strongest interaction remain as local as possible. To draw the analogy to the Hubbard model, most chemical systems would therefore correspond to the so-called small  $U$  limit.

The reordering concept can be put in a more rigorous form by minimizing the entanglement distance, which can be expressed as a cost function,

$$\hat{I}_{\text{dist}} = \sum_{i,j} I_{i,j} \times |i - j|^\eta, \quad (9)$$

where the entanglement between pair of sites is weighted by the distance in the chain between the orbitals. In

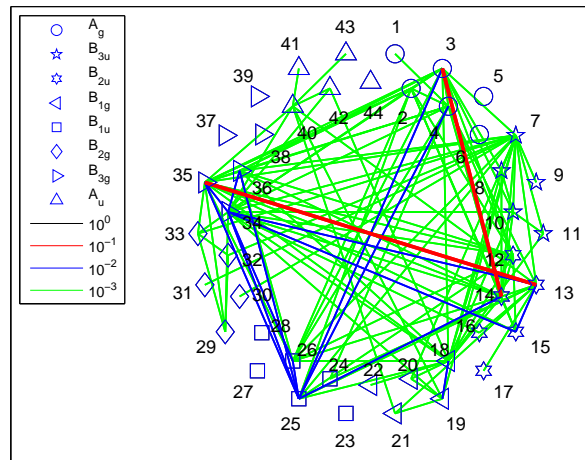


FIG. 4: (Color online) Components of the two-orbital mutual information which are larger than  $10^{-4}$  for the  $\mu - \eta^2 : \eta^2$  peroxo isomer of  $[\text{Cu}_2\text{O}_2]^{2+}$  obtained with  $\chi = 10^{-5}$  and for the energetical ordering. The role of symbols and numbers is the same as in Fig. 1.

Ref. [15], the effect of the parameter  $\eta = -2$  has been analyzed using simulated annealing. Additional parameters to weight the off-diagonal elements of  $I$  have been studied as well. In our approach, we use both  $\eta = 1$  and 2. The latter choice also has the advantage that it can be related to the spectral algorithms of seriation problems [52]. The main aim is to sequence a set of  $N$  objects, i.e., to bijectively map the elements to the integers  $1, \dots, N$  based on a real valued correlation function  $f(i, j) = f(j, i)$  which reflects the desire for items  $i$  and  $j$  to be near each other in the sequence. The two-orbital mutual information is such a function which can also be seen as a weighted graph. In general, the problem of finding all ways to sequence the elements, so that the correlations are consistent, becomes NP-complete [53] in the presence of inconsistencies. In such a case, there may be no consistent solution and one needs to find the best approximation. If a consistent ordering is possible, the problem is *well posed*. Most of the combinatorial algorithms for well-posed problems break down when the data is inconsistent, limiting their value for many problems. In our approach, the minimization is performed iteratively with the constraint that orbitals of the same irreducible representations are kept together, thus reordering of orbitals is allowed within irreducible representations and reordering the blocks of orbitals of the irreducible representation is also allowed. As a result, a highly optimized ordering can be obtained as is shown in Fig. 5. The value for the energetical ordering  $\hat{I}_{\text{dist}} = 821.4$  is reduced to 134.1 using  $\eta = 2$ . A smaller value of 63 could be reached by excluding the constraint discussed above. However, the DMRG calculations perform considerably worse for that ordering.

A further justification of our cost function can be dis-

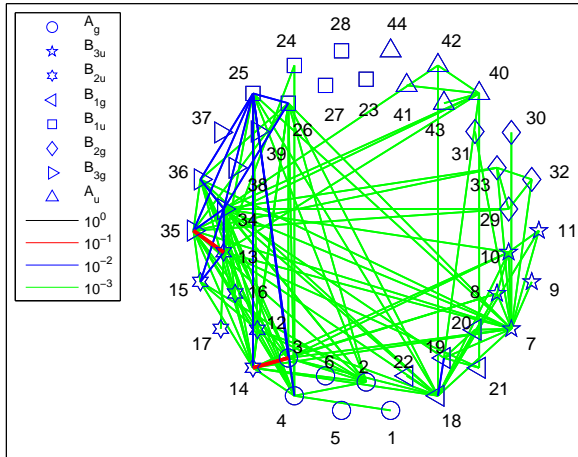


FIG. 5: (Color online) Similar to Fig. 4, but for the reordered orbitals.

cussed in terms of spectral algorithms. Since the minimization of the cost function  $g(\pi) = \sum_{i,j} f(i,j)(\pi_i - \pi_j)^2$  is hard in terms of permutations  $\pi$ , it can be approximated by a cost function like  $\hat{I}_{\text{dist}}$  of continuous variables  $x_i$  that maintains its structure. From spectral graph theory it follows that the so called Fiedler vector  $x = (x_1, \dots, x_N)$  is the solution that minimizes  $F(x) = x^\dagger L x = \sum_{i,j} I_{i,j}(x_i - x_j)^2$  subject to the following constraints that  $\sum_i x_i = 0$  and  $\sum_i x_i^2 = 1$ , where the graph Laplacian is  $L = D - I$  with  $D_{i,i} = \sum_j I_{i,j}$ . The second eigenvector of the Laplacian is the Fiedler vector [54, 55] which defines a (1-dimensional) embedding of the graph on a line that tries to respect the highest entries of  $I_{i,j}$  and the edge length of the graph. Ordering the entries of the Fiedler vector by non-decreasing or non-increasing way provides us a possible ordering. A naive application of optimization methods based on the Fiedler vector yielded a worse ordering than the one shown in Fig. 5. A more detailed analysis of energetical ordering based on the Fiedler vector will be part of our subsequent work. Numerical results obtained by the optimized ordering will be further discussed in Sec. IV.

Note that a new electronic wave function ansatz in terms of the complete-graph tensor network (CGTN) parametrization [10] might contain the same information as the weighted graph of the cost function in Eq. (9). This efficient parametrization might also be used to devise an optimized orbital ordering.

### E. Efficient calculation of the single-orbital entropy

The single-orbital entropy can be calculated for each renormalization step of a full sweep, thus  $s(1)_i$  can be obtained for  $i = 1 \dots N$ . Therefore, the single-orbital

entropy profile for a given ordering of molecular orbitals can be determined as a function of sweeps [13, 39]. Once the wave function has converged by means of the entropy sum rule [14], the single-orbital entropy profile for the given target state can be obtained. This well known procedure of collecting data points from subsequent renormalization steps of a full sweep was also used by Ghosh *et al.* to efficiently calculate four-point correlation functions [37]. The one-orbital entropy, on the other hand, can also be expressed in terms of the occupation-number representation [15]. Therefore, the calculation of  $s(1)_i$  is also possible once the required operators are determined for the given superblock configuration. A direct comparison of data points obtained by the two approaches provides a reliable error estimate.

### F. Efficient calculation of the two-orbital entropy function

The two-orbital entropy function can be expressed in terms of the occupation-number representation [15]. Unfortunately, it requires the calculation of 23 independent two-point correlation functions. Since all two-point correlation functions have to be renormalized and stored in memory or on disk due to the truncation of the superblock Hilbert space, the efficient calculation of these operators is crucial for feasible calculations with respect to wall time and computational resources.

In a standard real space DMRG procedure, the correlation functions are usually calculated for the symmetric superblock configuration, i.e., when the size of the left and right blocks are equal. This configuration provides the most accurate result for a fixed number of block states since the block entropy reaches its maximum value, so that the highest level of entanglement can be reached [14]. In fact, the largest error in a measurable quantity is related to the largest truncation error within a full DMRG sweep [56]. In contrast to this, using the DBSS method, the error can be kept below an a priori defined threshold, and hence an accurate calculation of the correlation functions is possible for the non-symmetric superblock configurations as well. In addition, if two non-interacting orbitals are attached to both ends of the chain the reduced block density matrix at the turning points of a sweep, where all orbitals belong to the left or the right block, has only one non-zero eigenvalue according to the Schmidt decomposition. Renormalized operators required for the two-orbital entropy function reduce to single numbers ( $M_l = M_r = 1$ ) [14, 39], consequently. Even without this trick, an efficient calculation of the correlation function at the turning points is possible because the environment block contains  $q$  basis states and the system block only  $M_{\text{min}}$  states when the DBSS procedure is used. This is crucial in the quantum information analysis since the construction of the mutual entropy is very costly. In our approach, all the required operators are generated only for the superblock configuration at the

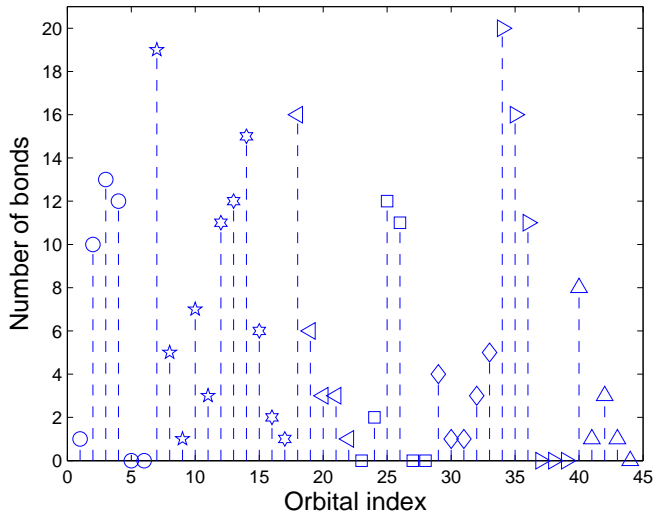


FIG. 6: (Color online) Number of entanglement bonds emerging from the orbitals based on Fig. 4. The meaning of the symbols is the same as in Fig. 2.

turning points for which the correlation functions are calculated. This is achieved by subsequent renormalization of the operators based on the a priori determined transformation matrices [30].

### G. Configuration Interaction based Dynamically Extended Active Space (CI-DEAS) procedure

The non-local version of the DMRG method is very sensitive to the initialization procedure. If a poorly approximated starting configuration is used, the convergence can be very slow and the DMRG can even be trapped in local minima [38]. This can, however, be avoided by including highly entangled orbitals from the very beginning and expanding the active space dynamically [13]. This approach has also been extended to include protocols based on the Configuration Interaction (CI) procedure [39, 40] and applied to systems with sizes up to 60 orbitals. Here, we briefly summarize the main aspects of the method as required for the discussion in this work.

Taking a look at Fig. 4, some orbitals are highly entangled with several other orbitals while others are entangled with a few orbitals only. The number of entanglement bonds emerging from the orbitals based on Fig. 4 is shown in Fig. 6.

In order to guarantee fast convergence the highly entangled orbitals — those with several entanglement bonds — should be included from the very beginning of the calculations. If the bonds are also weighted with their strength, by summing  $I$  column-wise, one gets back the diagonal entries of the graph Laplacian which corresponds to the single-orbital entropy. In the DEAS procedure,

we introduce a complete-active-space (CAS) vector that selects the highly entangled orbitals. The CAS vector (CASV) is formed by ordering orbitals with decreasing entropy values.

Since the DMRG algorithm itself is a basis-state transformation protocol, that transforms single-particle basis states to multi-particle basis states, the environment block in the DEAS procedure is formed for each DMRG iteration step from the one-particle basis states of those orbitals which possess the largest single-orbital entropies. In the first iteration step the left block (system block) contains one orbital represented by  $q$  states while the right block (environment block)  $r = N - l - 2$  orbitals. Since the exact representation of the right block would require  $q^{N-l-2}$  states which is too large for large systems, only a subset of orbitals is included to form the active space. Therefore, at each DMRG iteration step of the warm up procedure, i.e., for iterations  $1 \dots N - 3$  the  $M_r$  states are formed from those components of the CAS vector which belong to the environment block and possess largest entropies. The starting value of  $M_r$  ( $M_{\text{start}}$ ) is set prior of the calculation but during the iteration procedure  $M_r$  is adjusted as  $M_r = \max(M_l, M_{\text{start}})$  in order to construct at least as many environment states as the left block has in order to satisfy the constraints set by the Schmidt decomposition. Identifying orbitals of the right block as doubly filled, empty or active orbitals the effective size of the environment block can be reduced significantly. The empty orbitals can be neglected, while a partial summation over the doubly filled orbitals results in a constant shift in the energy. If DMRG auxiliary operators [57] are formed by partial summations on the left block, the effective system size of the problem is determined by the active orbitals only [13, 39, 40]. Therefore, in the warm up procedure the effective size of the system is reduced to 5 to 7 orbitals which allows one to use larger  $M_{\text{start}}$  without a significant increase in computational time.

In order to construct even better environment states, we also utilize CI expansion procedures. In standard CI techniques, the trial wave function is written as a linear combination of determinants with expansion coefficients determined by requiring that the energy should be minimized [58]. The molecular orbitals used for building the excited Slater determinants are taken from a CASSCF calculation and kept fix. Therefore, in the CI method the number of determinants included in the treatment is increased systematically in order to achieve a better accuracy. Determinants which are singly, doubly, triply, quadruply, etc. excited relative to the Hartree-Fock (HF) configuration are indicated by the subscripts  $S$ ,  $D$ ,  $T$ ,  $Q$ . The exact wave function in a given one-particle basis, the full-CI wave function, is then given as

$$\Psi_{\text{CI}} = a_0 \Phi_{\text{HF}} + \sum_S a_S \Phi_S + \sum_D a_D \Phi_D + \sum_T \phi_T \Phi_T + \dots \quad (10)$$

Since the segment of the HF-orbitals belonging to the environment block is known, the restricted subspace of

the environment block can be formed for a given CI-level in the DEAS procedure. Therefore, the right block contains states for a given CI-level while the total wave function can contain higher excitations as well due to the correlation between the two blocks. The environment block states are constructed at each iteration step, so that the environment block is always optimized for the renormalized system (left) block. This procedure guarantees that several highly entangled orbitals are correlated from the very beginning and both static and dynamic correlations are taken into account. The reduced density matrix is well defined, thus block states can be selected efficiently based on the entropy considerations and convergence to local minima can be avoided. Since a significant part of the correlation energy can be obtained in this way, usually at the end of the initialization procedure, i.e., after one-half sweep, chemical accuracy is often reached. The initial CAS vector can be determined based on the chemical character of the molecule or in a self-consistent fashion. In the latter approach, the CAS vector is set first as  $\text{CASV} = [N, N - 1, \dots, 1]$  to include long range interactions between the left block and the rightmost sites of the chain and a calculation using small values of  $M_{\min}$  and  $M_{\text{start}}$  is performed. After a full sweep, the entropy functions are calculated and the ordering as well as the CAS vector are determined. Even though the DMRG wave function has not yet converged, most relevant information of the system can already be extracted. In addition, the DMRG results can be systematically improved using the optimized ordering and the CAS vector as a starting point for new DMRG calculations. The CI-DEAS method allows a simple and fast calculation of all physical quantities at the end of the first sweep.

In the following section, the DBSS and CI-DEAS procedures are applied to chemical systems and the results are discussed in more detail.

#### IV. RESULTS

In this section, we present results for the two isomers of  $[\text{Cu}_2\text{O}_2]^{2+}$ . We discuss our DBSS/CI-DEAS procedures by analyzing the peroxo isomer while for the bis( $\mu$ -oxo) isomer only the final results will be given.

##### A. Electronic ground state of the two $[\text{Cu}_2\text{O}_2]^{2+}$ cores

Here, we summarize the main steps of our entropy-based optimization procedures. First, we perform a short DMRG calculation using a limited set of block states in order to obtain the most important characteristics of the entropy functions and to determine the low-lying energy spectrum. In order to use DMRG in an automated manner as a black-box method, we do not use any specific ordering or CAS vector related to the chemical characteristics of the problem.

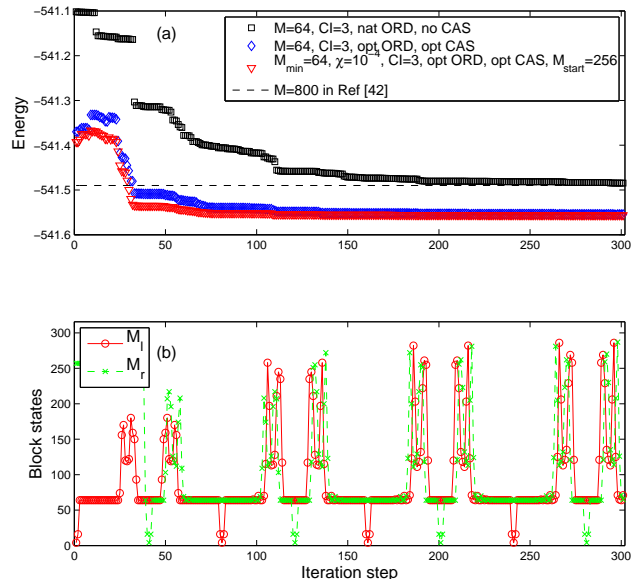


FIG. 7: (Color online) (a) Convergence of the ground state energy in Hartree for various parameters for the  $\mu - \eta^2 : \eta^2$  peroxo isomer. The dashed line gives the ground state energy obtained in Ref. [42] using  $M = 800$  block states. (b) Number of block states as a function of iteration steps for  $\chi = 10^{-4}$  corresponding to Fig. 9.

In order to determine the multiplicity of the converged target state, we also calculate the expectation value of the  $S^2$  operator given as

$$S^2 = \sum_{ij} S_i^- S_j^+ + \sum_{ij} S_i^z S_j^z + \sum_i S_i^z. \quad (11)$$

The expectation value is equal to  $S(S + 1)$  in Hartree atomic units, i.e., zero for a singlet state and two for a triplet state.

We performed a calculation with fixed  $M = 64$  states, using the energetical ordering, and the CAS vector was simply set to  $\text{CASV} \equiv [N, N - 1, \dots, 1]$ . This latter choice guarantees that during the initialization procedure long range interaction between the system block (left-block) and the rightmost sites of the chain is taken into account. In this calculation, we have restricted the CI-DEAS procedure to include determinants with at most triple excitations from the Hartree-Fock state. The convergence of the ground state energy in the  $A_g$  irreducible representation of the point group  $D_{2h}$  is shown in Fig. 7(a) as the square symbols. Although the convergence is rather slow, the results obtained in our previous work with  $M = 800$  block states [42] – shown by the dashed line – can be reached after eight sweeps. The convergence to the singlet state has been confirmed by the expectation value of the total-spin operator  $\langle S^2 \rangle = 10^{-3}$ .

The block entropy profile converges very slowly as shown in Fig. 8(b). In fact, the entropy profile cor-

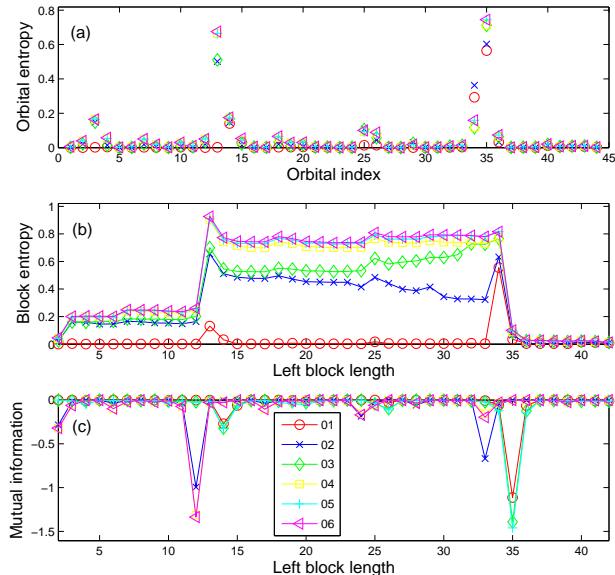


FIG. 8: (Color online)(a) Single-orbital entropy, (b) block entropy and (c) mutual information profile for the  $\mu - \eta^2 : \eta^2$  peroxo isomer of  $[\text{Cu}_2\text{O}_2]^{2+}$  using energetical ordering, without optimized CAS vector for the singlet ground state of  $A_g$  symmetry with fixed  $M = 64$  block states. The convergence of the ground state energy in Hartree is shown in Fig. 7(a) by the square symbol.

responding to the CI-DEAS procedure represented by the red circle symbol is almost zero for most of the superblock configurations which indicates the lack of entanglement between the DMRG blocks. As a consequence, the DMRG algorithm selected inappropriate states for the description of the environment blocks.

A detailed analysis of the entropy functions provides even better convergence properties. The obtained single-orbital and block entropies as a function of DMRG sweeps are shown in Fig. 8. By comparing Figs. 8(a) and 2, we see that orbitals with large entropies can already be identified and a reasonable CAS vector can thus be constructed. In Fig. 8(b), one also recognizes that once the third orbital is pushed in the left block, i.e., for  $l \geq 3$  the block entropy increases significantly. This is because the third orbital is highly entangled with the 14<sup>th</sup> and 25<sup>th</sup> orbitals as can be seen in Fig. 4. The largest values of the block entropy is reached for  $13 < l < 35$  when the highly entangled orbitals 13 and 35 belong to the two different blocks. In order to localize entanglement, ordering optimization based on the two-orbital mutual information can also be carried out according to the procedure described in Sec. II and a block entropy profile shown in Fig. 9(b) is obtained. By comparing Figs. 8(b) and 9(b) it is clear that in the latter case the block entropy is highly localized, i.e., it takes large values only for a few superblock configurations. Repeating the cal-

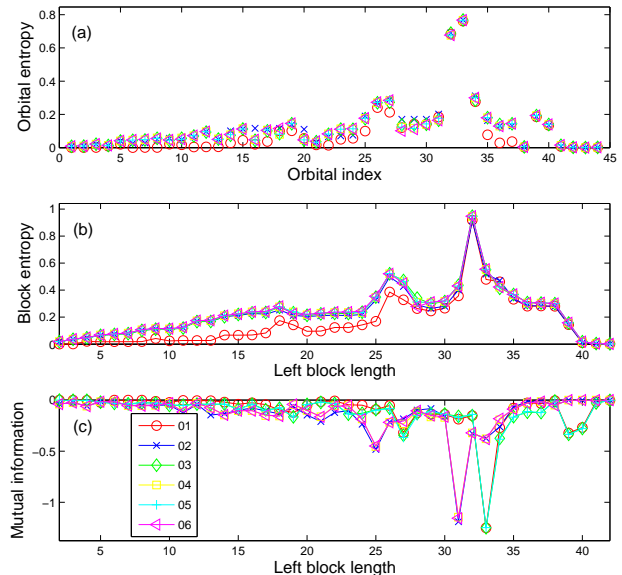


FIG. 9: (Color online)(a) Single-orbital entropy, (b) block entropy, and (c) mutual information obtained for the  $\mu - \eta^2 : \eta^2$  peroxo isomer of  $[\text{Cu}_2\text{O}_2]^{2+}$  as a function of DMRG sweeps with optimized ordering, CAS vector, and by setting the quantum information loss  $\chi = 10^{-4}$ . The CI-DEAS initialization procedure corresponds to symbols with red circle. The optimized ordering and CAS vector is given in Table I.

ulation with fixed  $M = 64$  block states again but using an optimized ordering and CAS vector yields a ground state energy estimate of  $E_{\text{peroxo}} = -541.55533$  Hartree. The fast convergence is shown in Fig. 7 by the diamond symbol. In fact, the ground state energy after the first half sweep, i.e., at the end of the CI-DEAS procedure is already far below the one given by Ref. [42] and the block entropy profile has the same structure as the one obtained after eight sweeps. This can be attributed to the CI-DEAS procedure for selecting the appropriate environment block states at each iteration step by taking care of the renormalized system block and the inclusion of the highly entangled orbitals from the beginning.

There is no need to use additional methods to guarantee convergence like white noise [25] or perturbative correction [43] which is an interesting observation in view of the results of Kurashige and Yanai. The optimized ordering and CAS vectors used in the calculation are summarized in Table I. Carrying out the same procedure for the bis( $\mu$ -oxo) isomer of  $[\text{Cu}_2\text{O}_2]^{2+}$ , the convergence of the ground state energy with fixed  $M = 64$  states without optimized ordering and CAS vector is shown in Fig. 10(a) by the square symbol. We also observe for the bis( $\mu$ -oxo) isomer, that our DMRG energies reproduce the results given in Ref. [42] with a fraction of the computational resources. It is clear that the convergence of the energy is very slow to the value given in Ref. [42], how-

---

ORD = [ 44 41 42 43 40 31 30 33 32 29 11 10 9 8 7  
 20 21 19 18 22 1 2 5 6 4 3 14 12 17 16  
 15 13 35 34 36 38 37 39 25 26 24 27 28 23 ]

CASV = [ 35 13 14 34 3 25 26 18 4 36 7 15 12 10 2  
 19 40 20 8 33 29 42 21 32 24 16 11 43 1 41  
 17 44 31 30 9 22 6 39 38 5 27 23 37 28]

---

TABLE I: Optimized ordering and CAS vector for the  $\mu-\eta^2$ :  $\eta^2$  peroxo isomer of  $[\text{Cu}_2\text{O}_2]^{2+}$ .

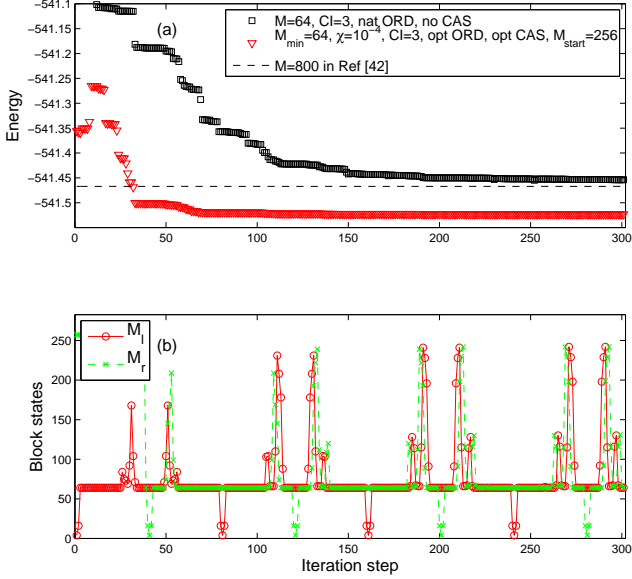


FIG. 10: (Color online) (a) Convergence of the ground state energy in Hartree for various parameters for the bis( $\mu$ -oxo) isomer. The dashed line gives the ground state energy obtained in Ref. [42] using  $M = 800$  block states. (b) Number of block states as a function of iteration steps for  $\chi = 10^{-4}$ .

ever, after the entropy-based optimization procedures, a much faster convergence to a much lower value can be reached. As a result, the optimized CAS vector based on the single-orbital entropy shown in Fig. 11 is given in Table II. The highly localized two-dimensional entanglement matrix for the optimized ordering is understood from the comparison of Figs. 12 and 13. The optimized ordering vector utilized in the calculation is given in Table II. The entanglement distance  $\hat{I}_{\text{dist}} = 1043$  for the energetical ordering is reduced to  $\hat{I}_{\text{dist}} = 102.5$  for the optimized ordering. The resulting entropy profiles as a function of sweeps are shown in Fig. 14. Again the block entropy takes large values only for a few iteration steps within a full sweep.

Since a very important observable related to transition metal clusters is the energy difference between the two isomers, the ground state energies should be calcu-

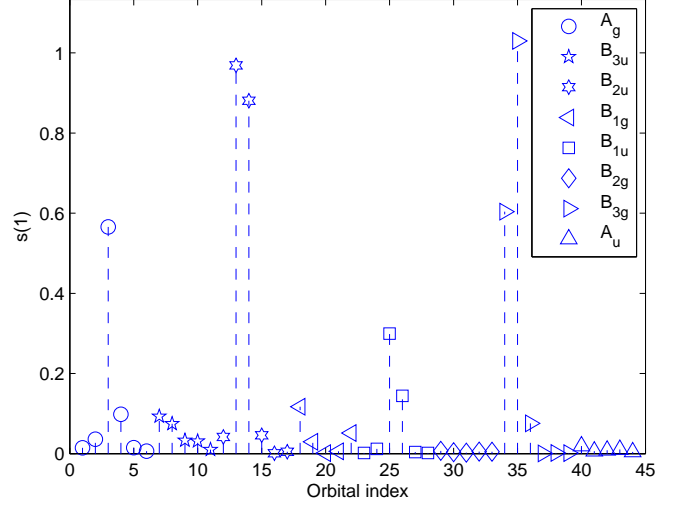


FIG. 11: (Color online) Similar to Fig. 2 but for the bis( $\mu$ -oxo) isomer of  $[\text{Cu}_2\text{O}_2]^{2+}$ .

---

ORD = [ 44 41 43 40 42 31 30 33 32 29 11 10 9 8 7  
 20 21 19 18 22 1 2 5 6 4 3 12 17 16 15  
 14 13 35 34 36 38 37 39 25 26 24 27 28 23 ]

CASV = [ 35 13 14 34 3 25 26 18 7 4 8 36 22 15 12  
 2 9 10 19 40 5 42 1 11 29 24 43 44 33 41  
 32 30 6 21 17 31 27 20 28 38 23 29 16 37 ]

---

TABLE II: Optimized ordering and CAS vector for the bis( $\mu$ -oxo) isomer of  $[\text{Cu}_2\text{O}_2]^{2+}$ .

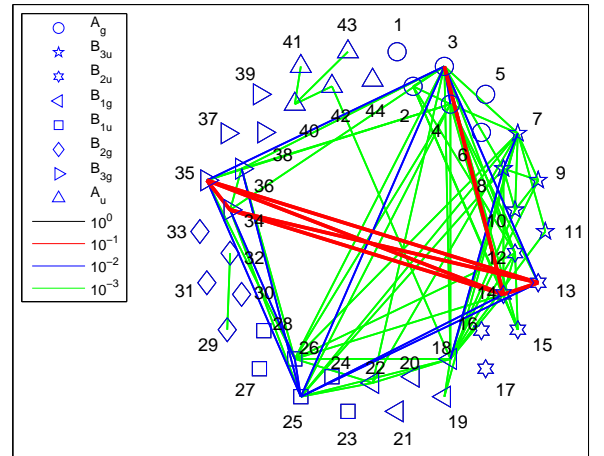


FIG. 12: (Color online) Similar to Fig. 4, but for the bis( $\mu$ -oxo) isomer of  $[\text{Cu}_2\text{O}_2]^{2+}$ .

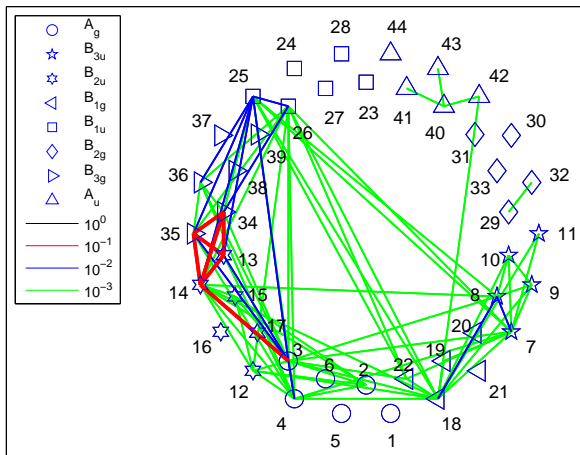


FIG. 13: (Color online) Similar to Fig. 12, but for the optimized ordering.

lated for the same error margin. This cannot be guaranteed with a fixed number of block states but it can be achieved by the DBSS procedure (or an automated Richardson-type error protocol [22]). We have thus calculated the ground state energies of the two isomers using the same parameter set, namely for  $M_{\min} = 64$ ,  $\chi = 10^{-4}$ ,  $M_{\text{start}} = 256$ . The convergence of the ground state energy is plotted in Fig. 7(a) by the triangle symbol, while the number of block states selected dynamically in Fig. 7(b). Since the block entropy is highly localized for the optimized ordering for most of the superblock configurations the number of block states were determined by  $M_{\min}$  as can be seen in Fig. 7(b) and Fig. 10(b). We found  $E_{\text{peroxo}} = -541.55628$  Hartree and  $E_{\text{bisoxo}} = -541.51416$  Hartree yielding an energy differences of 0.04212 Hartree, i.e., 110 kJ/mol. For both isomers we have obtained  $\langle S^2 \rangle = 10^{-4}$  for the ground state as expected from the given error margin.

The convergence of the ground state energy for the bis( $\mu$ -oxo) isomer is shown in Fig. 10(a) by the triangle symbol. The fast convergence is again evident. The effective size of the environment block during the first  $N$  iteration steps, i.e., for the CI-DEAS procedure, was found to be less than five orbitals. Therefore, using a larger number of block states for the environment block ( $M_{\text{start}}$ ) increases the computational time insignificantly. This result indicates that the application of DBSS and CI-DEAS procedures in the entropy-based optimization guarantees that the DMRG algorithm can be used in a black-box fashion, and that chemical accuracy can be reached using very limited computational resources. In fact, the reduced effective system size in the CI-DEAS procedure allows one to obtain the most relevant characteristics of the entropy functions within a few minutes.

To ensure that during the CI-DEAS procedure an even

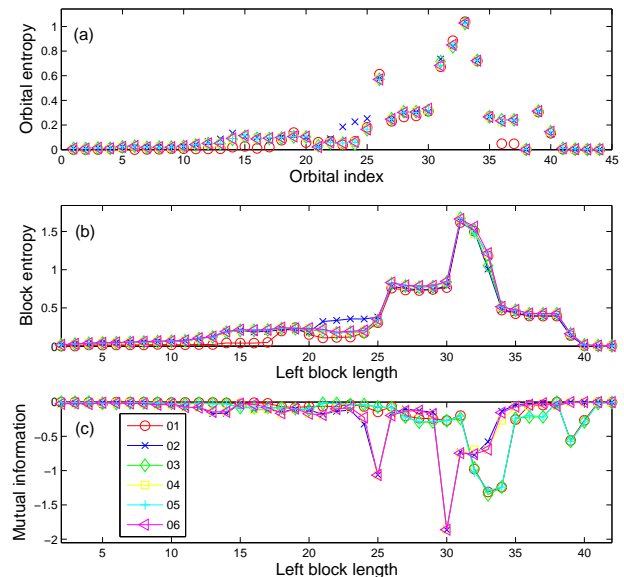


FIG. 14: (a) Single-orbital, (b) block-entropy, and (c) mutual information obtained for bis( $\mu$ -oxo) isomer of  $[\text{Cu}_2\text{O}_2]^{2+}$  as a function of DMRG sweeps with optimized ordering and CAS vector and for setting the quantum information loss to  $\chi = 10^{-4}$ . The CI-DEAS initialization procedure corresponds to symbols with red circle. The optimized ordering and CAS vector is given in the text.

better represented environment blocks are constructed, we have repeated the calculations using  $M_{\min} = 256$  and  $M_{\text{start}} = 1024$ . After eight sweeps, we obtained the following  $E_{\text{peroxo}} = -541.57900$  Hartree and  $E_{\text{bisoxo}} = -541.53599$  Hartree with a gap of 113 kJ/mol. In addition, we have performed more accurate calculations for  $\chi = 10^{-5}$ ,  $M_{\min} = 256$ , and  $M_{\text{start}} = 512$ . The maximum number of block states selected dynamically was around 1000 for the peroxo isomer, while for the bis( $\mu$ -oxo) isomer we found that slightly more states were required to reach the same accuracy, so that  $M_{\max}$  was in the range of 1200. In both calculations, we obtained  $\langle S^2 \rangle = 10^{-5}$  as expected for a singlet state. For the given error margin, we found  $E_{\text{peroxo}} = -541.58050$  Hartree,  $E_{\text{bisoxo}} = -541.53565$  Hartree, thus the difference is 0.04485 Hartree that is 118 kJ/mol.

In Table III, all relevant DMRG calculations for the bis( $\mu$ -oxo) and  $\mu - \eta^2 : \eta^2$  peroxo isomers of the binuclear copper cluster are listed. Total electronic energies of the two isomers reported by Malmqvist *et al.* [59] and Kurashige and Yanai [43] were calculated in a different active space. The latter authors then carried out new DMRG calculations [34], where they reduced their active space, but applied the canonical-transformation (CT) approach [33] and optimized the orbitals. A comparison of absolute energies is therefore not very meaningful as the total energy depends on the size of the CAS and the type

Ref.,method	$E_{\text{bisoxo}}$	$E_{\text{peroxo}}$	$\Delta E$
Reference energies			
[41],CASSCF(16,14)	-541.50307	-541.50345	1
[41],CASPT2(16,14)	-542.06208	-542.06435	6
[41],bs-B3LYP	-544.19419	-544.27844	221
[59],RASPT2(24,28)			120
Previously published DMRG energies			
[42],DMRG(26,44)[800]	-541.46779	-541.49731	78
[23],DMRG(26,44)[128]	-541.47308	-541.51470	109
[43],DMRG(32,62)[2400]	-541.96839	-542.02514	149
[34],DMRG(28,32)[2048]-SCF	-541.76659	-541.80719	107
[34],DMRG(28,32)[2048]-SCF/CT			113
DMRG energies from this work			
DMRG(26,44)[64/256/10 <sup>-4</sup> ]	-541.51416	-541.55628	111
DMRG*(26,44)[256/512/10 <sup>-4</sup> ]	-541.53499	-541.57896	115
DMRG*(26,44)[256/1024/10 <sup>-4</sup> ]	-541.53599	-541.57900	113
DMRG(26,44)[256/512/10 <sup>-5</sup> ]	-541.53565	-541.58050	118

TABLE III: The relative energies for the bis( $\mu$ -oxo) and  $\mu - \eta^2 : \eta^2$  peroxo  $[\text{Cu}_2\text{O}_2]^{2+}$  isomers obtained in this work and from previously published studies are listed in kJ/mol. All total energies are given in Hartree. The CAS is denoted in parentheses as '(electrons,orbitals)' while the information on DMRG block states  $M$  is given in brackets. Note that total energies for different CAS and different types of orbitals cannot be directly compared. All results from this work employ entropy-based optimization applying the DBSS and CI-DEAS procedures. The "\*" denotes keeping slightly more DMRG environment states during the initialization than necessary for a given quantum information loss  $\chi$ . The square brackets  $[M_{\text{min}}/M_{\text{start}}/\chi]$  state that the DMRG calculation starts with  $M_{\text{start}}$  block states, and the minimal number of block states is set to  $M_{\text{min}}$ , respectively.

of orbitals chosen. Instead we shall focus on the relative energy which is central to the chemistry of such systems. Our entropy-based DMRG calculations agree quantitatively with the RASPT2(24,28) and DMRG-SCF/CT calculations, even though no procedure — such as canonical transformation — has been employed to account for dynamical correlation in our studies. However, this is not surprising because Yanai *et al.* found [34] that the effect of CT is only about 4 kJ/mol in the given one-particle basis set. In the first study [42] on this problem we already found the relative DMRG energies converge faster than the absolute energies of each isomer. This finding has been confirmed by Yanai *et al.* [34].

It is evident from Table III that already our first DMRG estimate [42] for this relative energy was much closer than the CASSCF result to the correct splitting, which we may expect between 110 and 160 kJ/mol based on the RASPT2 calculation and the Kurashige–Yanai DMRG result for a much larger active space. Our improved result for the splitting [23], which we obtained for the original active space but with a reduced number of block states  $M_l = 128$  is with 109 kJ/mol already very

close to the DMRG-SCF/CT and RASPT2 results of 113 and 120 kJ/mol, respectively. Even the total energies turned out to be improved and in the case of the peroxo copper cluster below the small-CAS CASSCF result as it should be. In view of the fact that a discrepancy in relative energy of about 5 to 10 kJ/mol is acceptable for chemical accuracy, we emphasize that both results, 113 and 118 kJ/mol, are close and that hence already the small DMRG calculation is a feasible means to yield such relative energies.

## B. Entropic analysis of the two isomers

Besides the relative energies of the two isomers, one might deduce more information from the entropy functions related to the chemical properties of the binuclear copper cores. By comparing Figs. 2 and 11, it is clear that the importance of the orbitals is different for the two isomers as shown by the different distribution of the single-orbital entropy. In general, almost all orbitals possess some 10-20% larger entropy for the bis( $\mu$ -oxo) isomer but some of the orbitals have 2.5 – 3 times larger entropy than those of the peroxo isomer. For example, orbitals 3, 14, 34 produce much larger contributions to the total entanglement in case of the bis( $\mu$ -oxo) isomer. The total quantum correlation encoded in the ground state,  $I_{\text{Tot}} = \sum_{i=1,\dots,N} s(1)_i$ , is 3.49 and 5.39 for the  $\mu - \eta^2 : \eta^2$  peroxo and bis( $\mu$ -oxo) isomers, respectively. Thus, the bis( $\mu$ -oxo) isomer is more entangled which is also reflected by the larger maximum value of the block entropy for the bis( $\mu$ -oxo) isomer as can be seen by comparing Figs. 9 and 14.

The highly entangled molecular orbitals for the  $\mu - \eta^2 : \eta^2$  peroxo and bis( $\mu$ -oxo) isomers are shown in Figs. 15 and 16. The molecular orbital analysis shows that the highly entangled orbitals have an occupation number that strongly deviates from either being doubly occupied or empty. The entropy-based optimization scheme accurately determines those orbitals and thus allows one to perform efficient DMRG calculations with the smallest possible active space for a desired accuracy in the DMRG energy. The selected orbitals are close to the Fermi surface and would be included in a standard CASSCF calculation if one could employ these large active spaces as in DMRG calculations.

## V. SUMMARY AND PERSPECTIVE

### A. Relation to Tensor Network States

Our procedure has been demonstrated on a one-dimensional spatial topology related to the DMRG method, while the obtained two-dimensional entanglement matrix could be employed more efficiently in methods based on tensor network state (TNS) approaches. For example, the two-orbital mutual information can provide

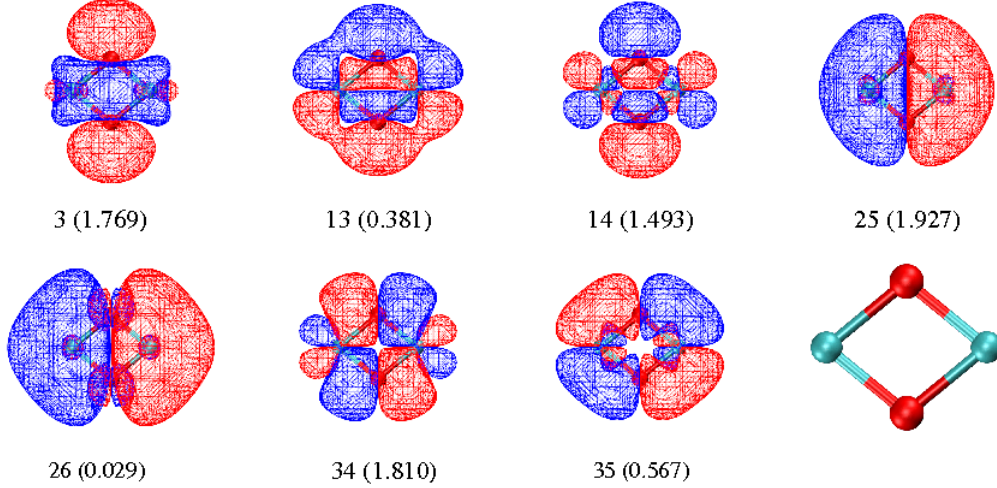


FIG. 15: (Color online) Molecular orbital pictures of the highly entangled orbitals for the bis( $\mu$ -oxo) isomer. The orbitals were selected with respect to their one-site entropy as shown in Fig. 11. The number below each orbital corresponds to the orbital index and the occupation number is written in the parentheses.

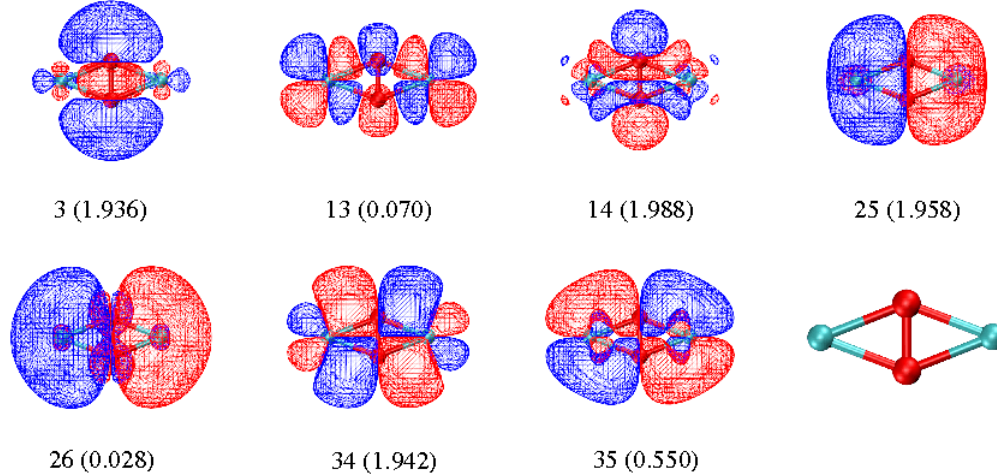


FIG. 16: (Color online) Molecular orbital pictures of the highly entangled orbitals for the peroxo isomer. The orbitals were selected with respect to their one-site entropy as shown in Fig. 2. The number below each orbital corresponds to the orbital index and the occupation number is written in the parentheses.

an optimal value for the coordination number of each orbital in case of the tree tensor network state (TTNS) approach [11] and an optimized network topology can be determined. Since in this latter method the distance between highly entangled orbitals can be reduced significantly compared to the DMRG topology entropy-based optimizations are expected to boost its convergence properties to a great extent. As an example, we present calculations performed with the TTNS method on the Be atom studied recently in Ref. [11]. The components of the two-orbital mutual information larger than  $10^{-4}$  are shown in Fig. 17(a). The convergence of the ground state

energy with a fixed bond dimension  $D = 2$  and coordination number  $z = 3$  for three different topologies shown in Fig. 18 is plotted in Fig. 17(b). It is found that for this set-up the relative error in the ground state energy dropped by an order of magnitude if an optimized topology based on the two-orbital mutual information is used. For the one-dimensional DMRG topology and for the energetical ordering, we found that  $\hat{I}_{\text{dist}} = 0.7251$  whereas it is reduced to 0.236 for the optimized topology of the TTNS method. For the topologies shown in Fig. 18 (a) and (b) we found a considerably larger values. We want to emphasize that for the one-dimensional

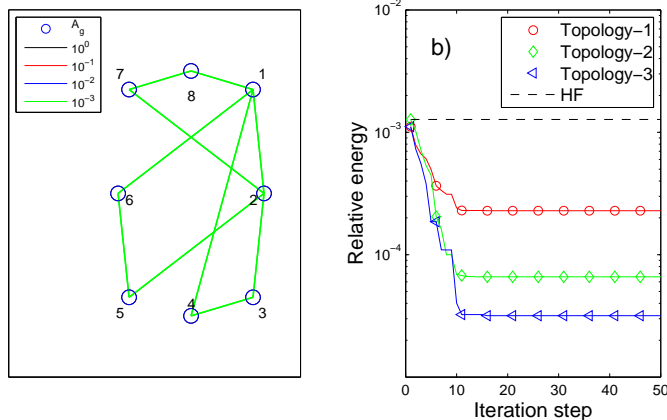


FIG. 17: (Color online) (a) Similar to Fig. 4, but for the Be atom. (b) Convergence of the ground state energy for the Be atom obtained with the TTNS method with a fixed bond dimension  $D = 2$  and coordination number  $z = 3$  for three different network topologies shown in Fig. 18 [60].

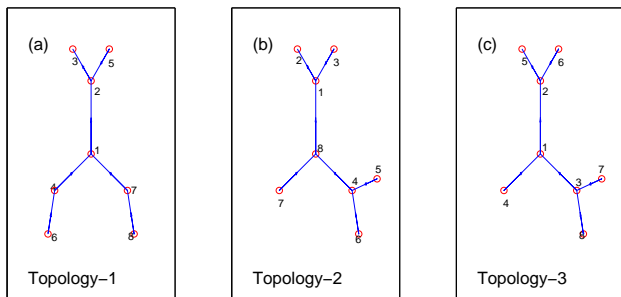


FIG. 18: (Color online) Three different network topologies were used for the TTNS method. The topology shown in (c) is optimized based on the two-orbital mutual information.

DMRG topology the lowest value of  $\hat{I}_{\text{dist}}$  is 0.30 by including all permutations of the orbitals. For the optimized ordering based on the Fiedler vector,  $\hat{I}_{\text{dist}}$  is 0.319 for which, in fact, we obtained the lowest ground state energy ( $E_{\text{rel}} = 1.69 \times 10^{-5}$ ) when fixed  $M = 8$  DMRG block states were used. A detailed study based on spectral analysis and graph theory and extension of our approach to larger systems is under progress and will be part of a subsequent work.

The optimization of the spatial arrangement of orbitals and network topologies has a significant influence on the convergence properties of MPS and TNS algorithms. However, the total entanglement encoded in the wave function,  $I_{\text{Tot}}$ , cannot be changed. The optimization of the one-particle basis can yield entanglement reduction in the system and the value of  $I_{\text{Tot}}$  can be manipulated, consequently. In fact, as discussed in Ref. [15] by constructing an optimal basis it might be that ordering is either obvious or irrelevant. In the past few years,

various procedures have been developed for orbital optimizations [11, 29, 32–37]. We will therefore continue to examine mutual information with respect to orbital optimization in our subsequent work.

## B. Conclusion

In this paper, we have studied a transition metal cluster from a quantum information theory perspective using the DMRG method. By calculating various entropy functions and the two-orbital mutual information we have proposed recipes to perform DMRG calculations in a black-box fashion on complex chemical compounds.

Optimizations based on the two-orbital mutual information can be related to graph theory and spectral analysis of seriation problems. Our cost function is interpreted in terms of the Fiedler vector of the graph Laplacian. Our results confirm the importance of taking entanglement among molecular orbitals into account and the usefulness of graph theory for carrying out efficient calculations. Chemical characteristics of the two isomers of  $[\text{Cu}_2\text{O}_2]^{2+}$  have also been analyzed and interpreted in terms of the entropy functions.

The present work confirms our previous findings that even small- $M$  DMRG calculations provide a qualitatively correct description of transition metal clusters as demonstrated in Ref. [23, 42].

Our results indicate that highly entangled orbitals form subgroups. Therefore, a coarse-graining approach might be possible which could be efficiently implemented by the multiscale-entanglement-renormalization ansatz (MERA) [8].

In future work, we shall explore the promising DBSS/CI-DEAS method in DMRG calculations on a set of test molecules featuring states whose relative energy is difficult to calculate. Also, additional options for improvement like extrapolation schemes [22] shall be investigated.

## Acknowledgments

This work was supported in part by Hungarian Research Fund (OTKA) through Grant Nos. K68340 and K73455. Ö. L. acknowledges support from the Alexander von Humboldt foundation. K. M. and M. R. gratefully acknowledge financial support through a TH-Grant (TH-26 07-3) from ETH Zurich. We thank A. Mai, R. M. Noack, and Cs. Nemes for very valuable discussions and V. Murg for performing calculations with the TTNS method on the Be atom. We would especially like to thank the Erwin-Schrödinger-Institut in Vienna for its hospitality during the Quantum Computation and Quantum Spin Systems workshop in 2009, the ETH Zurich and the Pauli Center for Theoretical Studies at ETH Zurich for its hospitality during the CECAM workshop of “Tensor network methods for quantum chemistry” in 2010,

where many fruitful discussion took place.

- 
- [1] L. Amico, R. Fazio, A. Osterloh, and V. Vedral, *Rev. Mod. Phys.* **80**, 517 (2008).
- [2] S. R. White, *Phys. Rev. Lett.* **69**, 2863 (1992).
- [3] S. R. White, *Phys. Rev. B* **48**, 10345 (1992).
- [4] F. Verstraete and J. I. Cirac, arXiv:cond-mat/0407066v1 (2004).
- [5] V. Murg, F. Verstraete, and J. I. Cirac, *Phys. Rev. A* **75**, 033605 (2007).
- [6] V. Murg, F. Verstraete, and J. I. Cirac, *Phys. Rev. B* **79**, 195119 (2009).
- [7] F. Verstraete, J. I. Cirac, and V. Murg, *Adv. Phys.* **57** (2), 143 (2008).
- [8] G. Vidal, *Phys. Rev. Lett.* **101**, 110501 (2008).
- [9] H. J. Changlani, J. M. Kinder, C. J. Umrigar, and G. K.-L. Chan, arXiv:0907.4646v3 [cond-mat.str-el] (2009).
- [10] K. H. Marti, B. Bauer, M. Reiher, M. Troyer, and F. Verstraete, arXiv:1004.5303v1 [physics.chem-ph] (2010).
- [11] V. Murg, F. Verstraete, Ö. Legeza, and R. M. Noack, arXiv:1006.3095v1 [cond-mat.str-el] (2010).
- [12] G. Vidal, *Phys. Rev. Lett.* **91**, 147902 (2003).
- [13] Ö. Legeza and J. Sólyom, *Phys. Rev. B* **68**, 195116 (2003).
- [14] Ö. Legeza and J. Sólyom, *Phys. Rev. B* **70**, 205118 (2004).
- [15] J. Rissler, R. M. Noack, and S. R. White, *Chem. Phys.* **323**, 519 (2006).
- [16] Ö. Legeza, F. Gebhard, and J. Rissler, *Phys. Rev. B* **74**, 195112 (2006).
- [17] Ö. Legeza, J. Sólyom, T. Tincani, and R. M. Noack, *Phys. Rev. Lett.* **99**, 087203 (2007).
- [18] I. Affleck, N. Laflorencie, and E. S. Sørensen, *J. Phys. A: Math. Theor.* **42**, 504009 (2009).
- [19] S. R. White and R. L. Martin, *J. Chem. Phys.* **110**, 4127 (1999).
- [20] U. Schollwöck, *Rev. Mod. Phys.* **77**, 259 (2005).
- [21] G. K.-L. Chan, J. J. Dorando, D. Ghosh, J. Hachmann, E. Neuscamman, H. Wang, and T. Yanai, in *Frontiers in Quantum Systems in Chemistry and Physics*, edited by Wilson, S and Grout, PJ and Maruani, J and DelgadoBarrio, G and Piecuch, P (2008), vol. 18 of *Prog. Theor. Chem. Phys.*, pp. 49–65, arXiv:0711.1398v1 [cond-mat.str-el].
- [22] K. H. Marti and M. Reiher, *Mol. Phys.* **108**, 501 (2010).
- [23] K. H. Marti and M. Reiher, *Z. Phys. Chem.* **224**, 583 (2010).
- [24] G. Moritz and M. Reiher, *J. Chem. Phys.* **126**, 244109 (2007).
- [25] G. K.-L. Chan and M. Head-Gordon, *J. Chem. Phys.* **116**, 4462 (2002).
- [26] Ö. Legeza, J. Röder, and B. A. Hess, *Phys. Rev. B* **67**, 125114 (2003).
- [27] G. K.-L. Chan and M. Head-Gordon, *J. Chem. Phys.* **118**, 8551 (2003).
- [28] Ö. Legeza, J. Röder, and B. A. Hess, *Mol. Phys.* **101**, 2019 (2003).
- [29] H. G. Luo, M. P. Qin, and T. Xiang, arXiv:1002.1287v1 [cond-mat.str-el] (2010).
- [30] S. Östlund and S. Rommer, *Phys. Rev. Lett.* **75**, 3537 (1995).
- [31] G. Moritz, B. A. Hess, and M. Reiher, *J. Chem. Phys.* **122**, 024107 (2005).
- [32] S. R. White, *J. Chem. Phys.* **117**, 7472 (2002).
- [33] T. Yanai and G. K.-L. Chan, *J. Chem. Phys.* **124**, 194106 (2006).
- [34] T. Yanai, Y. Kurashige, E. Neuscamman, and G. K.-L. Chan, *J. Chem. Phys.* **132**, 024105 (2010).
- [35] D. Zgid and M. Nooijen, *J. Chem. Phys.* **128**, 144116 (2008).
- [36] D. Zgid and M. Nooijen, *J. Chem. Phys.* **128**, 014107 (2008).
- [37] D. Ghosh, J. Hachmann, T. Yanai, and G. K.-L. Chan, *J. Chem. Phys.* **128**, 144117 (2008).
- [38] G. Moritz and M. Reiher, *J. Chem. Phys.* **124**, 034103 (2006).
- [39] Ö. Legeza and J. Sólyom, International Workshop on “Recent Progress and Prospects in Density-Matrix Renormalization“, Lorentz Center, Leiden University, The Netherlands (2004), <http://www.itp.uni-hannover.de/~jeckelm/dmrg/workshop/proceedings/>.
- [40] Ö. Legeza, CECAM workshop for “Tensor network methods for quantum chemistry“, ETH Zurich. (2010).
- [41] C. J. Cramer, M. Włoch, P. Piecuch, C. Puzzarini, and L. Gagliardi, *J. Phys. Chem. A* **110**, 1991 (2006).
- [42] K. H. Marti, I. Malkin Ondik, G. Moritz, and M. Reiher, *J. Chem. Phys.* **128**, 014104 (2008).
- [43] Y. Kurashige and T. Yanai, *J. Chem. Phys.* **130**, 234114 (2009).
- [44] S. R. White, *Phys. Rev. B* **72**, 180403 (2005).
- [45] M. Reiher, *Chimia* **63**, 140 (2009).
- [46] M. Reiher, *Faraday Disc.* **135**, 145 (2007).
- [47] M. Podewitz, M. T. Stiebritz, and M. Reiher, *Faraday Disc.* **148**, in press (2010).
- [48] K. H. Marti and M. Reiher, *Phys. Chem. Chem. Phys.* (2010), to be submitted.
- [49] K. Pierloot, in *Computational Organometallic Chemistry*, edited by T. R. Cundari (Marcel Dekker, New York, 2001), pp. 123–158.
- [50] H.-J. Werner, P. J. Knowles, R. Lindh, M. Schütz *et al.*, MOLPRO, a package of ab initio programs designed by H.-J. Werner and P. J. Knowles, version 2002.6. (2002).
- [51] K. Zyczkowski, P. Horodecki, A. Sanpera, and M. Lewenstein, *Phys. Rev. A* **58**, 883 (1998).
- [52] J. E. Atkins, E. G. Boman, and B. Hendrickson, *SIAM J. Comput.* **28**, 297 (1998).
- [53] D. S. Greenberg and S. C. Istrail, Technical report, Sandia National Labs. (1994).
- [54] M. Fiedler, *Czech. Math. Journal* **23**, 298 (1973).
- [55] M. Fiedler, *Czech. Math. Journal* **25**, 619 (1975).
- [56] Ö. Legeza and G. Fáth, *Phys. Rev. B* **53**, 14349 (1996).
- [57] T. Xiang, *Phys. Rev. B* **53**, R10445 (1996).
- [58] F. Jensen, *Introduction to computational chemistry* (Wiley, New York, 1999).
- [59] P. A. Malmqvist, K. Pierloot, A. R. M. Shahi, C. J. Cramer, and L. Gagliardi, *J. Chem. Phys.* **128**, 204109 (2008).
- [60] V. Murg (2010), unpublished results.